

Estimating electric current densities in solar active regions

M. S. Wheatland¹

© Springer ●●●●

Abstract Electric currents in solar active regions are thought to provide the energy released via magnetic reconnection in solar flares. Vertical electric current densities J_z at the photosphere may be estimated from vector magnetogram data, subject to substantial uncertainties. The values provide boundary conditions for nonlinear force-free modelling of active region magnetic fields. A method is presented for estimating values of J_z taking into account uncertainties in vector magnetogram field values, and minimizing J_z^2 across the active region. The method is demonstrated using the boundary values of the field for a force-free twisted bipole, with the addition of noise at randomly chosen locations.

Keywords: Active Regions, Magnetic Fields; Magnetic Fields, Models; Magnetic Fields, Corona

1. Introduction

The energy stored in active region magnetic fields produces large-scale solar activity, in particular solar flares. Flares often occur at sites in active regions overlying neutral lines where fields are strongly sheared, suggesting a connection between flares and large scale electric currents in the solar corona.

The most accurate determinations of active region magnetic fields and associated currents are based on measurements of the polarisation state of magnetically sensitive photospheric lines (del Toro Iniesta, 2003). The data are used to produce vector magnetograms, which are maps of the vector magnetic field $\mathbf{B} = (B_x, B_y, B_z)$ across regions on the photosphere (where x and y refer to the heliographic west and north directions respectively, and z is the radially outwards direction). The process of going from polarisation measurements to vector magnetogram values involves atmospheric modelling, the resolution of an intrinsic 180-degree ambiguity in the direction of the component of the field transverse to the line of sight, rotation of coordinate systems, and often also involves rebinning of the data. The resulting field values are substantially uncertain. Contributions to the uncertainty include errors in the original polarisation measurements, inaccuracy of the atmospheric model assumed in spectro-polarimetric inversion, errors in the ambiguity resolution, and loss of information in rebinning.

The measurement errors depend on the instrument, and two types of instruments are in use. Spectro-polarimeters record the full Stokes profile at many wavelengths across a magnetically sensitive spectral line, whilst magnetographs, or filter-based instruments, record polarisation signals integrated with respect to wavelength over a line

¹ SIfA, School of Physics, The University of Sydney, NSW 2006, Australia, email: m.wheatland@physics.usyd.edu.au

(Landi Degl’Innocenti and Landolfi, 2004). The Hinode Solar Optical Telescope (SOT) Focal Plane Package includes a Spectro-Polarimeter (Tsuneta et al., 2008), and the Helioseismic and Magnetic Imager on the Solar Dynamic Observatory (SDO) provides filtergrams (Scherrer *et al.*, 2012). Spectro-polarimeter typically have a high spectral resolution and provide very accurate measurements of the polarisation state, but they take longer to produce the data for a vector magnetogram and the magnetic field may change during the observation interval. Filter instruments produce data for a region on the Sun more rapidly, but they lack the spectral resolution and intrinsic high accuracy provided by a spectro-polarimeter.

Given a set of vector magnetic field values, estimates of the vertical (locally radial) electric current density at the level of the photosphere ($z = 0$) may be made using Ampère’s law:

$$\mu_0 J_z(x, y, 0) = v - u, \quad (1)$$

where we introduce the notation

$$u = \left. \frac{\partial B_x}{\partial y} \right|_{z=0} \quad \text{and} \quad v = \left. \frac{\partial B_y}{\partial x} \right|_{z=0}. \quad (2)$$

If the uncertainties in the field values are σ_x and σ_y , and centered differencing is used to estimate the derivatives, then the uncertainties in the derivatives are $\sigma_u = \sigma_x/\sqrt{2}h$ and $\sigma_v = \sigma_y/\sqrt{2}h$, where h is the grid spacing in the magnetogram in x and y . If the spatial scale for variation of the horizontal field is L , then we have $u \sim \overline{B}_x/L$ and $v \sim \overline{B}_y/L$, where \overline{B}_x and \overline{B}_y denote characteristic values of the field components. In that case

$$\frac{\sigma_u}{u} \sim \frac{L}{h} \frac{\sigma_x}{\overline{B}_x} \quad \text{and} \quad \frac{\sigma_v}{v} \sim \frac{L}{h} \frac{\sigma_y}{\overline{B}_y}. \quad (3)$$

Equations (3) imply that if there are significant fractional uncertainties in the field values, then the derivative estimates may be substantially uncertain, in particular for high-resolution data (with $L \gg h$). The current densities obtained using Equation (1) will be correspondingly uncertain.

Errors in the determination of current densities from vector magnetogram data were discussed by Pevtsov, Canfield, and Metcalf (1994) and Leka and Skumanich (1999), who assigned constant uncertainties for field components in the directions along, and transverse to, the line of sight. Uncertainty values may be assigned to individual vector magnetogram field values based on the quality of the model fit in the spectro-polarimetric inversion, and this information is now routinely supplied with vector magnetogram field values (e.g. Hoeksema *et al.*, 2014). Other sources of uncertainty have also been discussed, including errors in ambiguity resolution (Leka *et al.*, 2009), and errors introduced by the rebinning of data in the construction of magnetograms (Leka and Barnes, 2012).

The nonlinear force-free model is often used to model the coronal magnetic field based on vector magnetogram data (e.g. Wiegmann and Sakurai, 2012). The model is defined by $\text{curl } \mathbf{B} = \alpha \mathbf{B}$ and $\text{div } \mathbf{B} = 0$, where α is the force-free parameter. The Grad and Rubin (1958) method of solution of these equations takes as boundary conditions the values of B_z at the photosphere, and the values of J_z (or the values of α) over one polarity of B_z . Other methods, in particular the optimization method (e.g. Wheatland, Sturrock, and Roumeliotis, 2000, Wiegmann and Inhester, 2010), use all three components of \mathbf{B} at the photosphere as boundary conditions. In practice all methods modify the boundary data substantially from the values in the vector magnetogram in order to achieve a solution to the force-free model (see e.g. De Rosa *et al.*,

2009, Wheatland and Leka, 2011, Wiegelmann *et al.*, 2012). For the active region modelled by Wheatland and Leka (2011) using the ‘self-consistent’ Grad-Rubin procedure (Wheatland and Régnier, 2009), the current densities in the magnetogram were altered to the extent that the average absolute change in the horizontal field was 170 gauss, and the average ratio of the change in the horizontal field to the assigned uncertainty in the horizontal field, on a pointwise basis across the magnetogram, was ≈ 9 . The changes greatly exceeded the nominal uncertainties, which is typical. The ‘pre-processing’ procedure often used with the optimization method of nonlinear force-free solution (Wiegelmann, Inhester, and Sakurai, 2006) alters the transverse components of the field by $\lesssim 500$ gauss in strong field regions (Fuhrmann *et al.*, 2011). If nonlinear force-free codes are applied to vector magnetogram boundary data without these changes, accurate solutions to the nonlinear force-free model are (generally) not obtained.

The large changes required in vector magnetogram data to achieve nonlinear force-free model solutions are most likely due to the inconsistency of boundary data with the model (see e.g. Schrijver *et al.*, 2008, De Rosa *et al.*, 2009). The solar magnetic field is not expected to be force-free at the level of the photosphere. Errors in the field estimates also lead to inconsistency. Depending on the solution method, this problem may cause the solution magnetic fields to have significant departures from the divergence-free condition (Valori *et al.*, 2013).

In this paper we reconsider the problem of estimating electric current densities from vector magnetogram boundary data, taking into account uncertainties in the data. A method is introduced for calculating a set of boundary values of J_z which minimize departures from centred difference estimates for the current densities at locations where the values are accurate (according to the uncertainties), and which minimize the sum of J_z^2 across the magnetogram. The goal is an estimate of the current density which avoids large values produced by errors. The method is tested in application to a test case with known errors. The paper is divided as follows. Section 2 presents the method, and Section 3 describes the test and analyzes the results. Section 4 draws conclusions.

2. Method

Equation (1) provides the vertical current density in terms of the horizontal field gradients u and v . The problem consists in estimating the gradients from the data, subject to uncertainties, and we also seek to avoid large (spurious) values of the resulting vertical current densities, produced by points with large uncertainties. Hence we consider the problem of minimizing

$$F = \sum_{ij} \frac{(u_{ij} - u_{ij}^{\text{est}})^2}{2\sigma_{u\ ij}^2} + \frac{(v_{ij} - v_{ij}^{\text{est}})^2}{2\sigma_{v\ ij}^2} + \lambda \sum_{ij} J_z^2, \quad (4)$$

where the indices refer to points (x_i, y_j) in the magnetogram, u_{ij}^{est} and v_{ij}^{est} are estimates of the gradients, and where λ is a constant. It is useful to non-dimensionalize by expressing lengths, field strengths, and current densities in units of characteristic values B_s , L_s , and $B_s/\mu_0 L_s$, respectively. Using Equation (1), Equation (4) may be written in non-dimensional form

$$F = \sum_{ij} \frac{(u_{ij} - u_{ij}^{\text{est}})^2}{2\sigma_{u\ ij}^2} + \frac{(v_{ij} - v_{ij}^{\text{est}})^2}{2\sigma_{v\ ij}^2} + \Lambda \sum_{ij} (v_{ij} - u_{ij})^2, \quad (5)$$

where $\Lambda = \lambda B_s^2 / \mu_0 L_s^2$.

A minimum value of F is obtained when $\partial F / \partial u_{ij} = \partial F / \partial v_{ij} = 0$, which gives two coupled linear equations for the values of u_{ij} and v_{ij} corresponding to the minimum:

$$\begin{aligned} \frac{u_{ij}^{\min} - u_{ij}^{\text{est}}}{\sigma_{u_{ij}}^2} - 2\Lambda (v_{ij}^{\min} - u_{ij}^{\min}) &= 0 \\ \frac{v_{ij}^{\min} - v_{ij}^{\text{est}}}{\sigma_{v_{ij}}^2} + 2\Lambda (v_{ij}^{\min} - u_{ij}^{\min}) &= 0. \end{aligned} \quad (6)$$

The simultaneous solution of Equations (6) is given by

$$u_{ij}^{\min} = \frac{1}{d} \left[\left(\frac{1}{\sigma_{v_{ij}}^2} + 2\Lambda \right) \frac{u_{ij}^{\text{est}}}{\sigma_{u_{ij}}^2} + 2\Lambda \frac{v_{ij}^{\text{est}}}{\sigma_{v_{ij}}^2} \right] \quad (7)$$

and

$$v_{ij}^{\min} = \frac{1}{d} \left[2\Lambda \frac{u_{ij}^{\text{est}}}{\sigma_{u_{ij}}^2} + \left(\frac{1}{\sigma_{u_{ij}}^2} + 2\Lambda \right) \frac{v_{ij}^{\text{est}}}{\sigma_{v_{ij}}^2} \right], \quad (8)$$

where

$$d = \frac{1}{\sigma_{u_{ij}}^2 \sigma_{v_{ij}}^2} + 2\Lambda \left(\frac{1}{\sigma_{u_{ij}}^2} + \frac{1}{\sigma_{v_{ij}}^2} \right). \quad (9)$$

The current density corresponding to the gradients which minimize F is $J_{z_{ij}}^{\min} = v_{ij}^{\min} - u_{ij}^{\min}$, which evaluates to

$$J_{z_{ij}}^{\min} = \frac{J_{z_{ij}}^{\text{est}}}{1 + 2\Lambda \sigma_{J_{ij}}^2}, \quad (10)$$

where

$$J_{z_{ij}}^{\text{est}} = v_{ij}^{\text{est}} - u_{ij}^{\text{est}} \quad (11)$$

and

$$\sigma_{J_{ij}}^2 = \sigma_{u_{ij}}^2 + \sigma_{v_{ij}}^2. \quad (12)$$

Equation (10) provides a surprisingly simple solution to the problem: the current density at each point is reduced from the usual estimate by a factor

$$f_{ij} = (1 + 2\Lambda \sigma_{J_{ij}}^2)^{-1}, \quad (13)$$

so at points with larger uncertainties the current density is reduced more. We refer to Equation (10) as the ‘minimum current’ estimate for the current density.

In the following we use centered differences to provide the estimates of the gradients:

$$u_{ij}^{\text{est}} = \frac{B_x(x_i, y_j + h) - B_x(x_i, y_j - h)}{2h} \quad (14)$$

and

$$v_{ij}^{\text{est}} = \frac{B_y(x_i + h, y_j) - B_y(x_i - h, y_j)}{2h}, \quad (15)$$

where h is the grid spacing in the magnetogram in x and y . With these choices the uncertainties in the gradients, using propagation of errors, are

$$\sigma_{u\ ij} = \frac{1}{2h} (\sigma_{x\ ij+1}^2 + \sigma_{y\ ij-1}^2)^{1/2}, \quad (16)$$

and

$$\sigma_{v\ ij} = \frac{1}{2h} (\sigma_{y\ i+1j}^2 + \sigma_{y\ i-1j}^2)^{1/2}, \quad (17)$$

and the error in the current density is

$$\sigma_{J\ ij} = \frac{1}{\sqrt{2}h} (\sigma_{x\ ij+1}^2 + \sigma_{y\ ij-1}^2 + \sigma_{y\ i+1j}^2 + \sigma_{y\ i-1j}^2)^{1/2}. \quad (18)$$

Higher order differencing schemes are sometimes used. In the general case Equation (14) is replaced by

$$u_{ij}^{\text{est}} = \frac{1}{2h} \sum_k c_k B_x(x_i, y_j + kh), \quad (19)$$

where the sum enumerates the points involved in the differencing, and the c_k are coefficients. Equation (16) is replaced by

$$\sigma_{u\ ij} = \frac{1}{2h} \sum_k (\alpha_k^2 \sigma_{x\ ij+k}^2)^{1/2}, \quad (20)$$

and corresponding relations hold for v_{ij}^{est} and $\sigma_{v\ ij}$. Equation (18) is replaced by

$$\sigma_{J\ ij} = \frac{1}{2h} \left[\sum_k \alpha_k^2 (\sigma_{x\ ij+k}^2 + \sigma_{y\ ij+k}^2) \right]^{1/2}. \quad (21)$$

3. Test using simulated data

3.1. Boundary conditions and minimum current estimate

The method is demonstrated in application to a test case consisting of boundary conditions for a twisted bipole, with noise added to the boundary values at some points.

Panels (a), (b), and (c) of Figure 1 illustrate the twisted-bipole boundary conditions. Panel (a) shows the vertical component of the boundary field, $B_z(x, y, 0)$, which is constructed by adding the field from monopole sources at locations (x_+, y_+, z_+) and (x_-, y_-, z_-) . In non-dimensional units we have

$$B_z(x, y, 0) = C \left(\frac{z - z_+}{R_+^3} - \frac{z - z_-}{R_-^3} \right), \quad (22)$$

with

$$R_{\pm} = [(x - x_{\pm})^2 + (y - y_{\pm})^2 + z_{\pm}^2]^{1/2}, \quad (23)$$

and with C chosen such that $\max |B_z(x, y, 0)| = 1$. The boundary field is constructed over the region $0 \leq x \leq 1$ and $0 \leq y \leq 1$, with the choices $x_+ = 0.6$, $x_- = 0.4$,

$y_+ = y_- = 0.5$, and $z_+ = z_- = -0.2$. A current is introduced by assuming a boundary distribution of the force-free parameter α over the positive polarity of the field. We choose

$$\alpha(x, y, 0) = \begin{cases} \alpha_0 & \text{if } B_z \geq B_1 \\ 0 & \text{otherwise,} \end{cases} \quad (24)$$

with $B_1 = 0.9$ and $\alpha_0 = 15$. The boundary conditions on B_z and α are used to calculate a nonlinear force-free field in the cubical region defined by the boundary region and $0 \leq z \leq 1$, using the CFIT Grad-Rubin code (Wheatland, 2007). The calculation is performed on a $100 \times 100 \times 100$ grid. Panel (b) of Figure 1 shows the magnitude of the horizontal field

$$B_h(x, y, 0) = [B_x(x, y, 0)^2 + B_y(x, y, 0)^2]^{1/2} \quad (25)$$

for the calculated force-free field and panel (c) shows the corresponding values of the current density $J_z(x, y, 0)$ for the force-free field, estimated using Equation (1) with the centered difference values Equations (14) and (15) used for the field gradients. The patch of positive current matches the current density $J_z = \alpha B_z$ defined by the boundary conditions on B_z and α assumed for the force-free calculation [Equations (22) and (24)], and the patch of negative current density follows from the mapping of the boundary values of α along field lines in the force-free field.

Noise is added to the boundary values of \mathbf{B} from the force-free calculation, to provide a set of ‘observed’ boundary values. At a fraction θ of the boundary positions, randomly chosen, additional components δB_x and δB_y are added to $B_x(x, y, 0)$ and $B_y(x, y, 0)$ respectively, where δB_x and δB_y are normally distributed random numbers with mean zero and standard deviation $\sigma_x = \sigma_y = \sigma_0$, and where σ_0 is a chosen constant. The boundary values of $B_z(x, y, 0)$ are not altered. Panel (d) of Figure 1 illustrates the resulting noisy values of the horizontal field, for the choices $\theta = 0.1$ and $\sigma_0 = 0.25$, and panel (e) shows the corresponding current density, which we use for J_z^{est} . The values are obtained using Equation (1) applied to the observed (noisy) boundary values with centered differencing used to estimate the gradients. The noise in the horizontal field leads to spurious values of the current density, which mask the positive and negative patches seen in panel (c).

Panel (f) of Figure 1 shows the minimum current estimate J_z^{min} for the current density calculated using Equation (10) with the choice $\Lambda = 5$. This value of Λ was chosen because it reduces the noise in weak field regions to small values. The values of $J_z(x, y, 0)$ shown in panel (e) provide the estimate J_z^{est} , and the uncertainties in the current density values σ_J follow from Equations (16)-(17) assuming $\sigma_x = \sigma_y = \sigma_0$ at points with noise, and $\sigma_x = \sigma_y = 0$ at points without noise. Panel (f) shows that J_z^{min} returns a good approximation to the underlying distribution of current density in the boundary, except at locations affected by the noise in the horizontal field.

With the chosen value of Λ , the RMS value of $(J_z^{\text{est}} - J_z^{\text{min}})/\sigma_J$ over the boundary points with $\sigma_J > 0$ is close to unity. This is because the current density at the locations affected by noise is reduced by a value essentially equal to the noise. For this test case the minimum current estimate changes the boundary values within the uncertainties.

3.2. NLFFF reconstructions

The minimum current estimates for the current density enable reconstruction of a nonlinear force-free field. If the CFIT code is applied using the noisy current density estimates J_z^{est} the Grad-Rubin iteration does not converge: the noise in the data prevents a successful reconstruction. However, accurate force-free solutions are obtained using the minimum current estimate for the current densities.

Figure 2 illustrates the force-free solutions. Panel (a) shows the original NLFFF obtained from the boundary data without noise. The greyscale shows the boundary values of B_z , which are shown also in panels (b) and (d), and the white curves are a set of field lines originating at the positive pole. (Each of the panels in Figure 2 shows a cropped central region, by comparison with Figure 1.) Panel (b) shows the P and N solutions obtained from the boundary values of B_z together with the minimum current method estimates for current density. The white field lines correspond to the P solution, and the black field lines to the N solution. Panel (b) shows that the P and N solutions are twisted bipole configurations which are similar to the original field [panel (a)] and to each other, but are not identical. The P and the N solutions have less twist than the original field due to the reductions in current density at points affected by noise, and the energies of the fields are correspondingly decreased. The energy E of the original field shown in panel (a) is given by $E/E_0 = 1.083$, where E_0 is the energy of a potential field with the same lower boundary values for B_z [calculated by the method described for the CFIT code (Wheatland, 2007)]. The energies of the P and N solutions shown in panel (b) are given by $E_P/E_0 = 1.064$ and $E_N/E_0 = 1.048$. The reconstructed P and N fields contain about 80% and about 60% of the free magnetic energy of the original field, respectively.

We apply also the self-consistency procedure presented in Wheatland and Régnier (2009), which uses boundary values at both polarities to identify a single NLFFF solution. The procedure involves a cycle of calculations of P and N solutions. After a pair of solutions is calculated, the boundary values of α in the two solutions are averaged, taking into account uncertainties in the α values. The resulting averaged α values provide the boundary conditions for the P and N solutions in the next cycle. After a number of cycles, the P and N solutions agree, and provide a ‘self consistent’ solution. Panels (c) and (d) in Figure 2 illustrate the results. Panel (c) shows the P and N solutions – the white and black curves, respectively – after nine self-consistency cycles. The two sets of field lines are mostly overlapping. The energies of the P and N solutions are $E_P/E_0 = E_N/E_0 = 1.085$. A self-consistent solution is found, with a free energy a few percent higher than the energy of the original field. Panel (d) shows the J_z values in the self-consistent field, for comparison with panel (c) of Figure 1. The self-consistency procedure recovers a good approximation to the original set of current density values, although there are detailed differences. The method is able, to some extent, to ‘remove the noise’ because at a boundary point affected by noise, say at the P polarity, the uncertainty in the α value is large. The averaging procedure replaces this α value with the α value from the N solution, provided it has a much smaller uncertainty. This procedure generally recovers the original α values.

The self-consistent solution is qualitatively similar to the original field. A quantitative measure is provided by the mean vector error (Schrijver *et al.*, 2006):

$$E_m = \frac{1}{M} \sum_i \frac{|\mathbf{B}_{\text{orig},i} - \mathbf{B}_{\text{sc},i}|}{|\mathbf{B}_{\text{sc},i}|}, \quad (26)$$

where \mathbf{B}_{orig} is the original NLFFF, \mathbf{B}_{sc} is the field obtained by the self-consistency procedure, and $M = 100^3$ is the number of grid points. We find $E_m = 1.6 \times 10^{-2}$, indicating close correspondence.

4. Discussion and conclusions

A method is presented (the ‘minimum current’ method) for estimating vertical electric current densities J_z at the photosphere from vector magnetogram data. The procedure

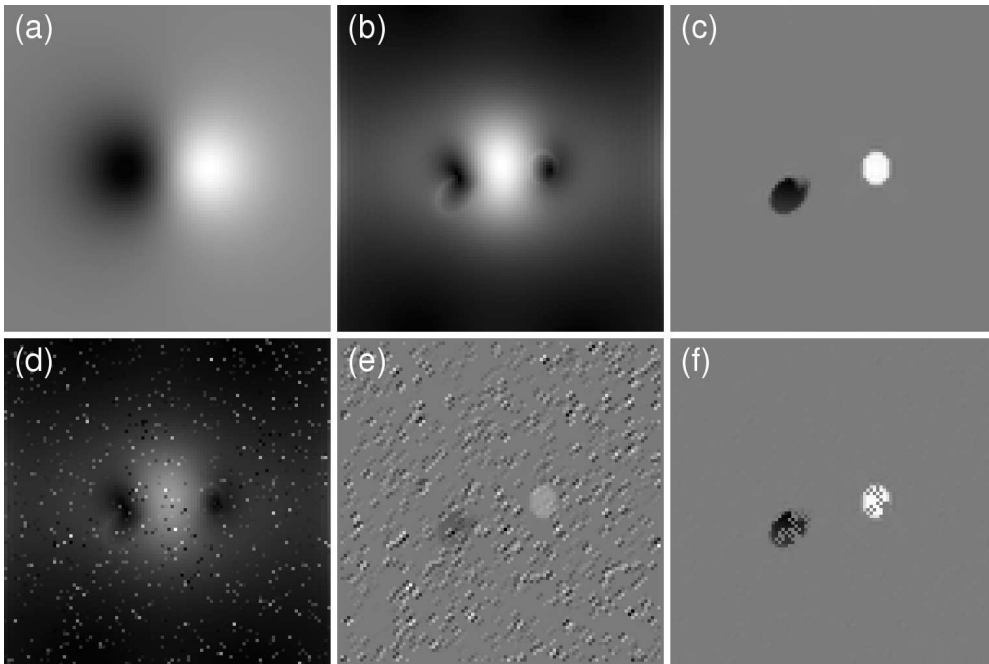


Figure 1. Application of the method to a simple bipole test case: boundary values. Panel (a) shows the boundary conditions on B_z for the test case and panel (b) shows the horizontal field in the boundary, obtained from a NLFFF solution with the chosen boundary conditions on B_z and current density. Panel (c) shows values of J_z in the boundary for the force-free field. Noise is introduced to the horizontal field values at a fraction of boundary locations, as shown in panel (d), which influences the estimated values for J_z [panel (e)]. Panel (f) is the minimum current estimate J_z^{est} for the vertical current density from the noisy boundary data.

alters the horizontal field gradients used to calculate the current densities subject to the uncertainties in the estimates for the field gradients, and also minimizes the sum of the square of the vertical current densities over all points in the magnetogram. The resulting minimum current estimate for the vertical current density at a given boundary location is reduced from the original estimate by a factor $1 + \Lambda\sigma_J^2$, where σ_J is the uncertainty in the original estimate of the current density, and Λ is a chosen constant which determines the relative importance of adherence to the original current density estimate or minimization of the sum of J_z^2 over all boundary locations.

The minimum current method provides an estimate for the current density which preserves values of the current density at locations with small uncertainties, and reduces the current density at locations with large uncertainties. The nonlinear force-free (NLFFF) model is often applied to vector magnetogram data to provide a proxy coronal field (e.g. Wiegmann and Sakurai, 2012). The construction of an accurate solution to the model requires modification of the boundary data from observed magnetogram values (e.g. Schrijver *et al.*, 2008, De Rosa *et al.*, 2009). The minimum current method may provide a more systematic approach to this modification.

A demonstration of the method is presented, in application to boundary field values for a NLFFF twisted bipole field configuration, with noise of a known amplitude added at a fraction of boundary locations. The model field values are taken to represent observed data with known uncertainties. The minimum current method recovers a good approximation to the original current density values in the boundary from the noisy data, except at locations affected by the noise. The method alters the boundary values

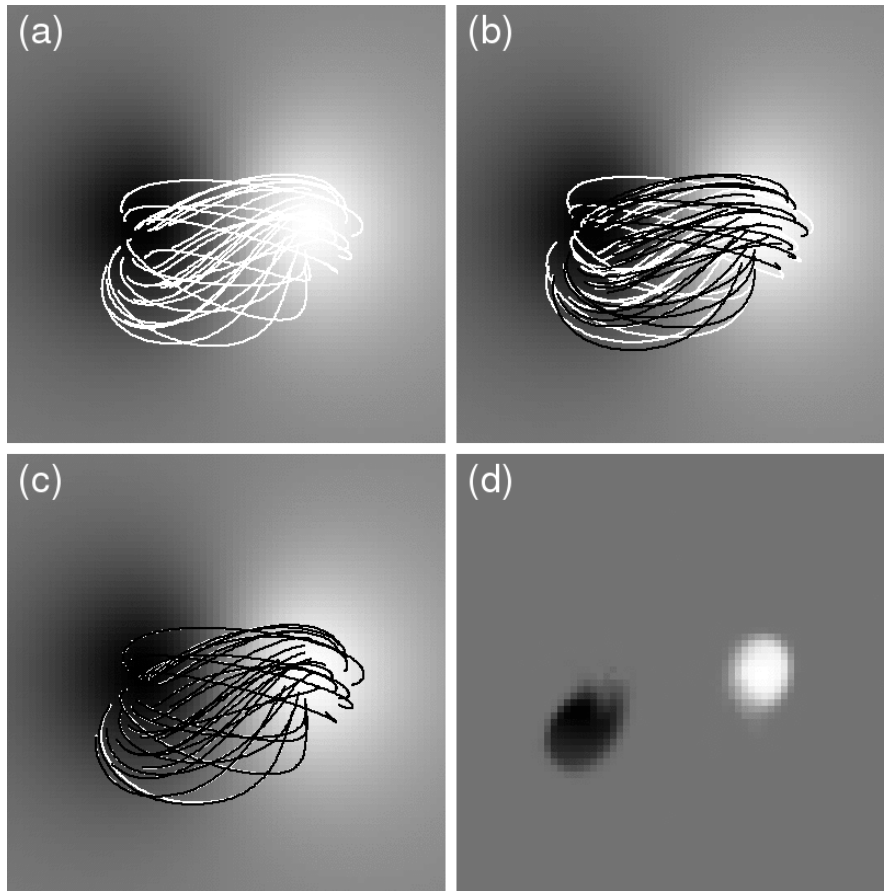


Figure 2. Application of the method to a simple bipole test case: nonlinear force-free fields. Panel (a) shows a set of field lines for the force-free field calculated from the original bipole boundary data, originating at the positive pole. Panel (b) shows comparable sets of field lines for the P solution (white lines) and for the N solution (black lines), calculated from the bipole values of B_z together with the minimum current method estimates J_z^{\min} for the current density over the P and N polarities of the field in the boundary, respectively. Panel (c) shows the solutions obtained with the Wheatland and Regnier (2009) self-consistency procedure (the white/black field lines show the P/N solutions at the end of a set of self-consistency cycles). Panel (d) shows the boundary values for current density in the self-consistency solution. The images in each panel are cropped to a central region in the computational domain, to more clearly show the field lines.

for current density within the uncertainties. The minimum current method boundary values are shown also to enable NLFFF reconstructions. The P and N solutions obtained from the boundary values are twisted bipole field configurations similar to the original NLFFF, but with reduced energies, due to the reduction in the boundary current density at locations affected by the noise. The self-consistency procedure (Wheatland and Régner, 2009) is applied, and demonstrated to produce a field which is a close match to the original NLFFF. The energy of the self consistent solution is within a few percent of the energy of the original NLFFF. The self-consistency procedure uses information on current density over both polarities of the boundary field, and hence is able to recover current density values affected by noise at one or other polarity.

We have chosen to minimize J_z^2 across the vector magnetogram to produce boundary data suitable for NLFFF modeling. The vertical current density is a boundary condition for the force-free model, and large estimates of J_z from vector magnetogram data

(which may be due to observational errors) can prevent NLFFF codes from producing an accurate force-free solution. However, this choice may remove or reduce local current concentrations which are real, and which contribute significantly to the energy of the field. Methods of resolving the 180-degree ambiguity used to produce vector magnetograms may also exclude real currents in the data (e.g. Metcalf, 1994; Metcalf *et al.*, 2006; Leka *et al.*, 2009). An advantage of the present method is that, if the uncertainties associated with currents are small, the currents are preserved. The accuracy of the minimum current estimate depends on the accuracy of the uncertainties provided.

The test of the method presented here is highly idealised. It is not intended to provide a realistic example of the application of the method to vector magnetogram data, but only to demonstrate the method, and to show its performance in the best case.

The method of inclusion of noise in the boundary data (adding Gaussian noise of known amplitude at specific locations to the horizontal field components of a NLFFF calculated from analytic boundary conditions) does not produce a close approximation to real solar data. We have not (yet) confronted the challenge of estimating electric currents from solar data with the minimum current method. Other studies have examined the influence of noise in vector magnetogram data (Wiegelmann *et al.*, 2010; Leka and Barnes, 2012). These studies add noise to synthetic line profiles, and then apply the various steps involved in constructing vector magnetograms (inversion, ambiguity resolution, co-ordinate transformations and rebinning, etc.). This process accurately mimics the influence of measurement errors on vector magnetograms. Tests of the method on data of this kind may be tried in future.

The current density estimates presented here use centered differences, but higher order differencing schemes could in principle be used, following Equations (14)–(21). High order schemes offer advantage in estimating gradients when applied to well-sampled data with small uncertainties, but the advantage is lost in application to sparse data, or data with substantial errors, and these schemes have the disadvantage of introducing correlations in the neighbouring estimates. As such we have chosen to use centered differences.

In future work the method will also be applied to vector magnetogram boundary data. This will allow investigation of whether the method is of use for coronal magnetic field modeling.

Acknowledgments The author thanks the referee, Thomas Wiegelmann, for comments which helped improve this paper.

References

- del Toro Iniesta, J.C.: 2003, *Introduction to Spectropolarimetry* ISBN 0521818273. Cambridge University Press, Cambridge.
- De Rosa, M.L., Schrijver, C.J., Barnes, G., Leka, K.D., Lites, B.W., Aschwanden, M.J., *et al.*: 2009, *Astrophys. J.* **696**, 1780, doi:10.1088/0004-637X/696/2/1780.
- Fuhrmann, M., Seehafer, N., Valori, G., and Wiegelmann, T.: 2011, *Astron. Astroph.* **526**, AA70, doi:10.1051/0004-6361/201015453.
- Grad, H., Rubin, H.: 1958, *Proc. 2nd Int. Conf. Peaceful Uses of Atomic Energy*, **31**, 190.
- Hoeksema, J. T., Liu, Y., Hayashi, K., *et al.* 2014, *Solar Phys.*, 289, 3483, doi:10.1007/s11207-014-0516-8.
- Landi Degl’Innocenti, E. and Landolfi, M.: 2004, *Polarization in Spectral Lines*, Dordrecht, Kluwer, 625.
- Leka, K.D., Barnes, G., Crouch, A.D., Metcalf, T.R., Gary, G.A., Jing, J., and Liu, Y.: 2009, *Solar Phys.* **260**, 83, doi:10.1007/s11207-009-9440-8.
- Leka, K.D. and Barnes, G.: 2012, *Solar Phys.* **277**, 89, doi:10.1007/s11207-011-9821-7.

- Leka, K.D. and Skumanich, A.: 1999, *Solar Phys.* **188**, 3, doi:10.1023/A:1005108632671.
- Metcalf, T.R.: 1994, *Solar Phys.* **155**, 235, doi:10.1007/BF00680593
- Metcalf, T.R., Leka, K.D., Barnes, G., Lites, B.W., Georgoulis, M.K., Pevtsov, A.A., Balasubramaniam, K.S., Gary, G.A., Jing, J., Li, J., Liu, Y., Wang, H.N., Abramenko, V., Yurchyshyn, V., and Moon, Y.-J.: 2006, *Solar Phys.* **237**, 267, doi:10.1007/s11207-006-0170-x.
- Pevtsov, A.A., Canfield, R.C., and Metcalf, T.R.: 1994, *Astrophys. J.* **425**, L117, doi:http://dx.doi.org/10.1086/187324.
- Scherrer, P. H., Schou, J., Bush, R. I., Kosovichev, A. G., Bogart, R. S., Hoeksema, J. T., Liu, Y., Duvall, T. L., Zhao, J., Title, A. M., Schrijver, C. J., Tarbell, T. D., Tomczyk, S.Z.: 2012, *Solar Phys.* **275**, 207. doi:10.1007/s11207-011-9834-2.
- Schrijver, C.J., De Rosa, M.L., Metcalf, T.R., Liu, Y., McTiernan, J., Régnier, S., Valori, G., Wheatland, M.S., and Wiegmann, T.: 2006, *Solar Phys.* **235**, 161, doi:10.1007/s11207-006-0068-7.
- Schrijver, C.J., De Rosa, M.L., Metcalf, T.R., Barnes, G., Lites, B., Tarbell, T., *et al.*: 2008, *Astrophys. J.* **675**, 1637, doi:10.1086/527413.
- Tsuneta, S., Ichimoto, K., Katsukawa, Y., Nagata, S., Otsubo, M., Shimizu, T., Suematsu, Y., Nakagiri, M., Noguchi, M., Tarbell, T., Title, A., Shine, R., Rosenberg, W., Hoffmann, C., Jurcevich, B., Kushner, G., Levay, M., Lites, B., Elmore, D., Matsushita, T., Kawaguchi, N., Saito, H., Mikami, I., Hill, L. D., and Owens, J. K.: 2008, *Solar Phys.* **249**, 167, doi:10.1007/s11207-008-9174-z.
- Valori, G., Démoulin, P., Pariat, E., and Masson, S.: 2013, *Astron. Astroph.* **553**, AA38, doi:10.1051/0004-6361/201220982.
- Wheatland, M. S., Sturrock, P. A., and Roumeliotis, G.:2000, *Astrophys. J.*, **540**, 1150, doi:10.1086/309355.
- Wheatland, M. S.: 2007, *Solar Phys.*, **245**, 251, doi:10.1007/s11207-007-9054-y.
- Wheatland, M.S. and Leka, K.D.: 2011, *Astrophys. J.* **728**, 112, doi:10.1088/0004-637X/728/2/112.
- Wheatland, M.S. and Régnier, S.: 2009, *Astrophys. J.* **700**, L88, doi:10.1088/0004-637X/700/2/L88.
- Wiegmann, T. and Inhester, B.: 2010, *Astron. Astroph.* **516**, AA107, doi:10.1051/0004-6361/201014391.
- Wiegmann, T., Inhester, B., and Sakurai, T.: 2006, *Solar Phys.* **233**, 215, doi:10.1007/s11207-006-2092-z.
- Wiegmann, T., Yelles Chaouche, L., Solanki, S.K., and Lagg, A.: 2010, *Astron. Astroph.* **511**, AA4, doi:10.1051/0004-6361/200912812.
- Wiegmann, T. and Sakurai, T.: 2012, *Living Reviews in Solar Physics* **9**, 5, <http://www.livingreviews.org/lrsp-2012-5>.
- Wiegmann, T., Thalmann, J.K., Inhester, B., Tadesse, T., Sun, X., and Hoeksema, J.T.: 2012, *Solar Phys.* **281**, 37, doi:10.1007/s11207-012-9966-z.